Film Evaporation from a Micro-Grooved Surface—An Approximate Heat Transfer Model and Its Comparison with Experimental Data

X. Xu* and V. P. Carey†
University of California, Berkeley, Berkeley, California 94720

An analytical model is presented that can be used to predict the heat-transfer characteristics of film evaporation on a microgroove surface. The model assumes that the liquid flow along a "V"-shaped groove channel is driven primarily by the capillary pressure difference due to the receding of the meniscus toward the apex of the groove, and the flow up the groove side wall is driven by the disjoining pressure difference. It also assumes that conduction across the thin liquid film is the dominant mechanism of heat transfer. A correlation between the Nusselt number and a nondimensional parameter Ψ is developed from this model which relates the heat transfer for the microgroove surface to the fluid properties, groove geometry, and the constants for the disjoining pressure relation. The results of a limited experimental study of the heat transfer during vaporization of a liquid coolant on a microgroove surface are also reported. Film-evaporation transfer coefficients inferred from these experiments are found to correlate fairly well in terms of Nusselt number and Ψ parameter format developed in the model. The results of this study suggest that disjoining pressure differences may play a central role in evaporation processes in microgroove channels.

Nomenclature

A = constant in the disjoining pressure equation
A_Δ = cross-sectional area of meniscus triangular channel, Eq. (4)
B = constant in the disjoining pressure equation
d_h = hydraulic diameter of the meniscus channel, Eq. (4)
f = Fanning friction factor
F_v = viscous term defined in Eq. (1)
G = mass flux in x direction
g = gravitational acceleration
h = heat transfer coefficient
h_{fg} = latent heat
K = parameter in Eq. (3)
k_f = thermal conductivity of liquid
L = length of the groove channel
$\dot{m}$ = mass flow rate in z direction
$\dot{m}_c$ = mass flow rate in x direction
N = number of grooves per unit length of surface
P_l = pressure in liquid region
P_v = pressure in vapor region
q'' = heat flux normal to the prime surface
q''_L = heat flux normal to the groove side walls
Re = Reynolds number
R_m = thermal resistance at the interface
R_δ = thermal resistance of the thin film
$r(x)$ = radius of meniscus at x
w = half of groove width
x = coordinate along groove channel
x_{max} = dryout location
y = coordinate normal to groove side wall
z = coordinate along groove side wall
z_m = maximum length of liquid film on groove side wall
β = slope of the groove surface with regard to gravity
δ = film thickness
η = nondimensional form of x coordinate, x/L
θ = half the vertex angle of a groove
μ_f = absolute viscosity of liquid
ν_f = kinematic viscosity of liquid
Ψ = nondimensional parameter, $w/r(x)$
ρ_f = density of liquid
σ = surface tension
$\bar{\sigma}$ = condensation coefficient

Received Feb. 13, 1989; revision received Sept. 29, 1989.

*Research Assistant, Department of Mechanical Engineering.
†Associate Professor, Department of Mechanical Engineering.

Introduction

EVAPORATION of thin liquid films has long been recognized as a means of achieving high heat transfer coefficients and/or high heat flux densities. As a result, techniques which employ this mechanism have considerable potential for use in a number of technical applications, including heat pipes for aerospace thermal control, electronics cooling, desalination systems, and process heat exchangers (see, for example, Ref. 1). One means of creating such a thin film is to promote the formation of an extended meniscus at the location where a liquid free surface contacts a solid wall. Experimental studies on the evaporation of the two-dimensional extended meniscus have been conducted by Renk and Wayner,[2] Cook et al.,[3] Wayner et al.,[4] and Mirzamoghadam and Catton.[5] These researchers used optical techniques to explore the film-thickness variation and transport in the liquid film during the evaporation process.

Analytical models of evaporation from the meniscus and/or extended thin film have also been presented in several studies. Potash and Wayner[6] have studied the evaporation from an extended two-dimensional meniscus. They applied the concept of disjoining pressure to the extended thin-film region above the intrinsic meniscus. Wehrle and Voulelikas[7] have presented a model for a similar scenario. However, in their model, a nonevaporating thin film was assumed to exist at the location where the intrinsic meniscus terminates, and the effect of disjoining pressure variations was ignored in this model.

Schneider et al.[8] have analyzed heat transfer in a "V"-groove channel and its walls using a finite element method. Edwards et al.[9] have presented a power-law solution for evaporation from a finned surface. They accounted for the variation in the curvature of the meniscus when computing the pressure gradient in the liquid. In 1979, Holm and Goplen[10] developed an analytical model for heat transfer in capillary grooves. An aim of this study was to assess the effects of interline heat transfer by varying several parameters such as groove spacing and heat input. In these calculations, the grooves were assumed to be rectangular, 0.508 mm wide and 1.27 mm deep. It was concluded that most of the heat was transferred in the intrinsic meniscus region while very little occurred in the evaporating film region.

In another study, Vasiliev et al.[11] performed experiments in which liquid flowed along "V"-shaped grooves placed horizontally. The maximum heat fluxes were obtained for different vertex angles and channel lengths.

The preceding studies provide valuable information on the mechanisms of evaporation from meniscus and/or thin films. However, the studies of evaporation in grooved channels just noted did not consider the interaction between a capillary-driven flow along a channel in a grooved surface and evaporation in the extended meniscus region at a given location. Such a circumstance is commonly encountered in heat-pipe evaporators such as those tested by Holmes and Feild.[1] In the investigation summarized here, the heat transfer mechanisms associated with microgroove evaporation processes of this type are considered in detail.

Moreover, several of the studies[7-9] did not consider the effect of disjoining pressure. The nature of the disjoining pressure effect described by Potash and Wayner[6] suggests that the rapid change in the film thickness at the interline near the end of the intrinsic meniscus would induce a large pressure gradient in the liquid (which can be calculated from the disjoining pressure equation given in Ref. 6). The pressure gradient induced by this mechanism may have a strong effect on the flow of liquid in this region.

The present investigation specifically focused on a surface with V-shaped microgrooves, similar to that considered by Holmes and Feild.[1] The grooves on these surfaces are of much smaller scale than those considered in the studies of Holm and Goplen[10] and Vasiliev et al.[11] An approximate analytical model of the flow and evaporative heat transfer in the microgrooves is presented. Our model differs from those developed in the preceding previous studies in that disjoining pressure effects are postulated to play a major role in the flow of liquid in the extended meniscus.

The disjoining difference across the film is known to vary directly with liquid film thickness.[6] In the interline region, the liquid film thickness is expected to vary strongly with distance along the wall of the V groove. This suggests that strong disjoining pressure gradients in the liquid may exist in this region, which may have a significant effect on the liquid motion there. The main objective of this study was to test this hypothesis against experimental evidence. The results of new heat transfer experiments for evaporation of methanol and acetone on a microgroove surface are also presented and used to evaluate the analytical model. Predictions of the model are also compared to data presented by Holmes and Feild[1] for evaporation of ammonia in a heat-pipe evaporator.

Analytical Model

This analysis considers the microgroove geometry shown in Fig. 1. One end of the V-shaped microgroove is immersed in a pool of the testing liquid. The liquid is assumed to "wick" up; the groove against gravity and/or a frictional pressure gradient by establishing a varying radius of curvature at the interface of the intrinsic meniscus. The intrinsic meniscus recedes closer to the apex of the groove to achieve this reduction in the radius of curvature. In addition, it is assumed that liquid is adsorbed onto the groove wall, forming an extended thin film above the intrinsic meniscus (see Fig. 1).

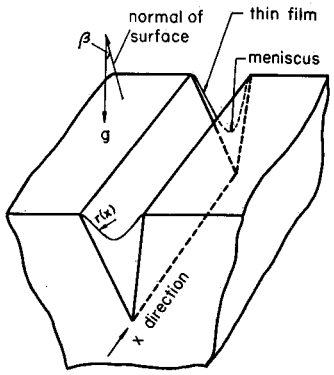

Fig. 1 Intrinsic meniscus and thin-film profiles along the groove channel.

The analysis is carried out based on the following idealizations: 1) The axial flow along the groove channel (in the x direction) occurs mainly in the intrinsic meniscus region, because the resistance to flow in the thin film is higher; 2) the intrinsic meniscus has a constant radius of curvature at a certain x, and the capillary pressure gradient due to the decreasing radius drives the liquid flow in the x direction; 3) the curvature effect is neglected in the extended thin-film region, and the disjoining pressure gradient due to the variation of film thickness drives the film flow up the V-groove wall (in the z direction); 4) evaporation occurs primarily in the thin-film region, and the heat transfer across the thin film is by conduction along; 5) the vapor pressure is constant.

We first consider the axial flow (in the x direction), as indicated in Fig. 1. The force balance equation for flow in the x direction is given by

$$\frac{dP_l}{dx} + \rho_f g \sin\beta + F_v = 0 \tag{1}$$

where β is the angle between the gravity direction and the normal of the prime surface. Here, F_v, the viscous term, is related to the Fanning friction factor f as

$$F_v = \frac{2fG^2}{\rho_f d_h} \tag{2}$$

where f for an open channel flow of this type has been determined by Ayyaswamy et al.[12] to be given by

$$f = \frac{K}{Re}, \qquad Re = \frac{Gd_h}{\mu_f} \tag{3}$$

In the above relation for f, K depends on the groove half-angle θ and the contact angle. Note that K in Eq. (3) is one-fourth of the value given in Ref. 12 due to the differences in the definition of f. By neglecting the axial liquid flow in the thin-film region and assuming that the contact angle of the meniscus is zero, as depicted in Fig. 2, A_Δ and d_h are given by

$$A_\Delta = c_1 r^2(x), \qquad d_h = c_2 r(x) \tag{4}$$

where

$$c_1 = \frac{1}{\tan\theta} - \left(\frac{\pi}{2} - \theta\right), \qquad c_2 = 2c_1 \tan\theta$$

Since P_v is constant, we can, in light of the capillary equation, relate the liquid pressure gradient to the radius of curva-

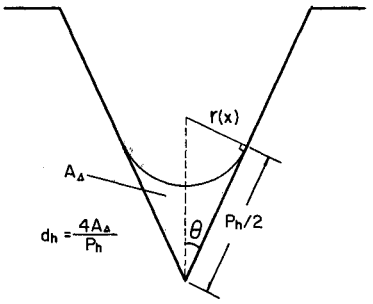

Fig. 2 Geometry of the assumed meniscus triangular channel.

ture as

$$\frac{dP_l}{dx} = -\frac{d}{dx}(P_v - P_l) = -\frac{d}{dx}\left(\frac{\sigma}{r(x)}\right) \tag{5}$$

Combining Eqs. (1-5), and noting that by definition $G = \dot{m}_c/A_\Delta$, we convert Eq. (1) to

$$\frac{d}{dx}\left(\frac{\sigma}{r(x)}\right) = \rho_f g \sin\beta + \frac{2K\dot{m}_c v_f}{c_3 r^4(x)} \tag{6}$$

where $c_3 = c_1 c_2^2$. For a specified $q''(x)$, if the liquid is saturated, $\dot{m}_c$ is given by

$$\dot{m}_c = -\frac{1}{Nh_{fg}}\int_{x_{max}}^{x} q''(x)\,dx \tag{7}$$

where $\dot{m}_c$ is zero at x_{max}.

Substituting Eq. (7) into Eq. (6), and introducing the following nondimensional variables

$$\eta = \frac{x}{L}, \qquad \Psi = \frac{w}{r(x)}, \qquad Q''(\eta) = c_4 q''(x) \tag{8}$$

where

$$c_4 = \frac{2Kv_f L^2}{c_3 w^3 N\sigma h_{fg}}$$

a differential equation for Ψ can be obtained

$$\frac{d\Psi}{d\eta} = -\Psi^4\int_{\eta_{max}}^{\eta} Q''(\eta)\,d\eta + c_5 \sin\beta \tag{9}$$

where

$$c_5 = \frac{\rho_f g L w}{\sigma}$$

Assuming that $r(x)$ is equal to $w/\cos\theta$ at $x = 0$, (i.e., the meniscus fills the entire V groove), we obtain

$$\Psi = \cos\theta, \qquad \text{at } \eta = 0 \tag{10}$$

Solving Eqs. (9) and (10) for $\Psi(\eta)$, we may obtain the radius of curvature of the meniscus as a function of x for a given $q''(x)$.

We subsequently consider the flow up the groove wall (along the z axis), intending to determine the film-thickness profile on the groove side wall. In general, both capillary and disjoining pressure effects may play a role in determining the film thickness on the side walls of the V groove. However, this situation is idealized here by assuming that the capillary pressure only affects the intrinsic meniscus region, whereas disjoining pressure only affects the extended thin-film region. The pressure variation due to these effects must match at the junction of the intrinsic meniscus and the thin film.

As shown in Fig. 3, assuming the flow in the extended thin-film region is laminar, we can obtain the pressure gradient by making the z-direction force-momentum balance for an element of unit width

$$\frac{dP_l}{dz} = -\frac{3\dot{m}v_f}{\delta^3} - \rho_f g\cos\beta\cos\theta \tag{11}$$

As just postulated, the driving force in the thin liquid film is due to the gradient in the disjoining pressure. Following Potash and Wayner,[6] the relation between the disjoining pressure and the film thickness can be represented by

$$P_d = P_l - P_v = -A\delta^{-B} \tag{12}$$

where A and B are empirical parameters. As shown in Fig. 4, the relations for mass and energy conservation require that

$$d(-\dot{m}h_{fg}) = -q_L''\,dz \tag{13}$$

The z variation of the heat flux q_L'' is not known a priori. As a first approximation, we therefore idealize it as being uniform along the portion of the groove wall covered by the extended thin film. From Fig. 4, it can be seen that q_L'' and q_L'' must be related as

$$q_L''(2z_m) = q''(1/N) \tag{14}$$

The heat transfer to the intrinsic meniscus is expected to be small compared to that across the thin film and is thus neglected. Figure 4 also shows the relation between the maximum length of the film region z_m and radius of the meniscus, given by

$$z_m = \frac{w}{\sin\theta} - r(x)\cot\theta \tag{15}$$

Assuming $\dot{m} = 0$ at the top of the side wall ($z = 0$), we obtain

$$\dot{m} = \int_0^{\dot{m}} d\dot{m} = \frac{q''}{2Nh_{fg}}\left(\frac{z}{z_m}\right) \tag{16}$$

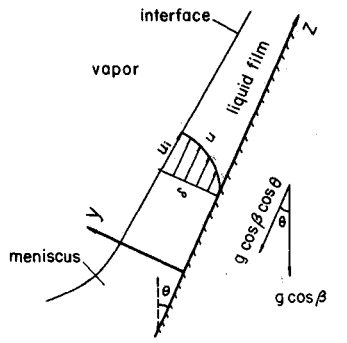

Fig. 3 Force balance schematic for the thin film on a groove side wall.

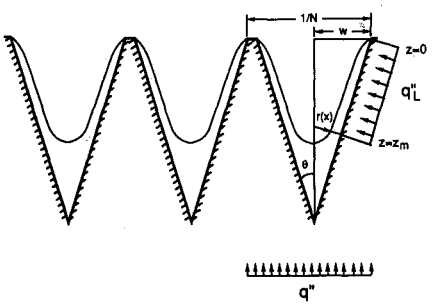

Fig. 4 Definition of two heat fluxes q_L'' and q'' with reference to the profiles of the intrinsic meniscus and the extended thin film.

Substituting Eqs. (16) and (12) into Eq. (11), the following differential equation for the film thickness is obtained

$$\frac{d\delta}{dz} = -\frac{\delta^{B+1}}{AB}\left[\frac{3v_f}{\delta^3}\left(\frac{q''}{2Nh_{fg}}\right)\left(\frac{z}{z_m}\right) + \rho_f g \cos\beta \cos\theta\right] \quad (17)$$

A boundary condition for this equation is obtained by matching the liquid pressure in the intrinsic meniscus region to that in the extended thin-film region at the junction of these two regions

$$(P_c)_{\text{meniscus}} = \frac{\sigma}{r(x)} = -(P_d)_{\text{film}} = A\delta_m^{-B}, \qquad \text{at } z = 0 \quad (18)$$

This matching thus yields

$$\delta = \delta_m = \left(\frac{Ar(x)}{\sigma}\right)^{1/B}, \qquad \text{at } z = 0 \quad (19)$$

The film-thickness variation in the z direction can be determined by numerically solving Eq. (17) using Eq. (19).

Since it is assumed that heat conduction across the thin film is dominant, and that the thermal resistance at the liquid-vapor interface is neglected, it follows that the heat transfer coefficient distribution along the groove can be determined from

$$h_L(x) = \frac{k_f}{z_m}\int_0^{z_m} \frac{dz}{\delta(x,z)} \quad (20)$$

The measured heat transfer coefficient is based on the base (projected) area of the groove surface; hence, we have

$$h(x) = (2z_m N)h_L(x) = 2k_f N\int_0^{z_m} \frac{dz}{\delta(x,z)} \quad (21)$$

By defining the following nondimensional parameters

$$\delta' = \frac{\delta}{w}, \qquad z' = \frac{z}{z_m} \quad (22)$$

Eqs. (19) and (21) can be transformed to

$$\frac{d\delta'}{dz'} = -\left(\frac{1}{\sin\theta} - \frac{\cot\theta}{\Psi(\eta)}\right)\left[\frac{c_6 Q''(\eta)}{\delta'^3}z' + c_7\cos\beta\right]\delta'^{B+1} \quad (23)$$

$$\delta' = \delta'_m = c_8\Psi^{-1/B}, \qquad \text{at } z' = 0 \quad (24)$$

where

$$c_6 = \frac{1}{c_4}\left(\frac{3w^{B-2}v_f}{2NABh_{fg}}\right), \quad c_7 = \frac{\rho_f g\cos\theta}{AB}w^{B+1}, \quad c_8 = \frac{1}{w}\left(\frac{Aw}{\sigma}\right)^{1/B}$$

and

$$h(\eta) = \frac{2k_f z_m N}{w}\int_0^1 \frac{dz'}{\delta'(\eta,z')} \quad (25)$$

For a specified coolant, groove geometry, heat flux variation $q''(x)$, and system vapor pressure, the preceding model can thus be used to predict the variation of the average heat transfer coefficient along the microgroove, provided that the disjoining pressure constants A and B are known.

At each x location along the groove, the nondimensional parameter Ψ is computed using Eq. (9). At the same time, the Nusselt number can be obtained from

$$Nu = \frac{h(\eta)w}{k_f} = 2z_m N\int_0^1 \frac{dz'}{\delta'(\eta,z')} \quad (26)$$

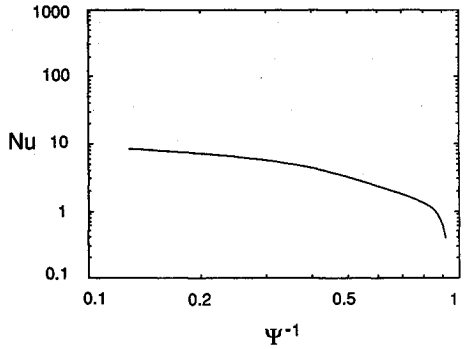

Fig. 5 Nusselt number vs Ψ^{-1} for methanol, obtained from the analytical model with the constants in the disjoining pressure relation $A = 1 \times 10^{-11}\ Pa(m)^B$ and $B = 3.0$.

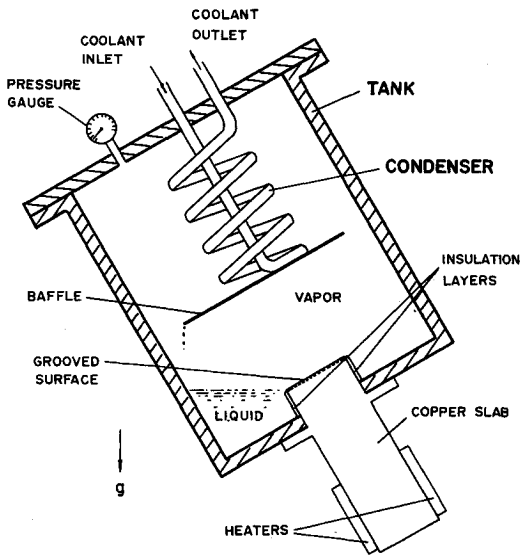

Fig. 6 Schemtaic of the test rig.

The relation between Nu and Ψ can then be determined for a specified groove geometry and test liquid. For the groove geometry considered in this study, the computed relation is shown in Fig. 5. The test liquid was methanol, and the constants A and B were chosen to be $A = 1.0 \times 10^{-11}\ Pa(m)^B$ and $B = 3.0$, respectively, where B is recommended in Ref. 6.

To examine the accuracy of this model, experiments were conducted in which the evaporative heat transfer performance of a microgroove geometry was determined for conditions such as those specified in the model calculations described above. The apparatus, procedure, and results of these experiments are described in the next two sections.

Experimental Apparatus

A schematic of the test rig used in the grooved-surface experiments is shown in Fig. 6. Parallel microgrooves were machined on one end of an oxygen-free copper slab, forming the testing surface. The copper slab was mounted at the bottom of a cylindrical, stainless steel tank with the grooved end inside the tank. At the opposite end of the copper slab, two electrical resistant heaters were clamped to either side to provide heat input. The heat input was virtually uniform at the same x location for different grooves (see Fig. 4).

As shown in Fig. 6, small portions of the side surfaces of the copper slab extended slightly into the tank. These areas were covered by a layer of plastic rubber to insulate the side wall against lateral heat loss. This ensured that virtually all of the heat would be directed to the grooved end surface. Flanges at both the top and the bottom of the tank were sealed using O-rings.

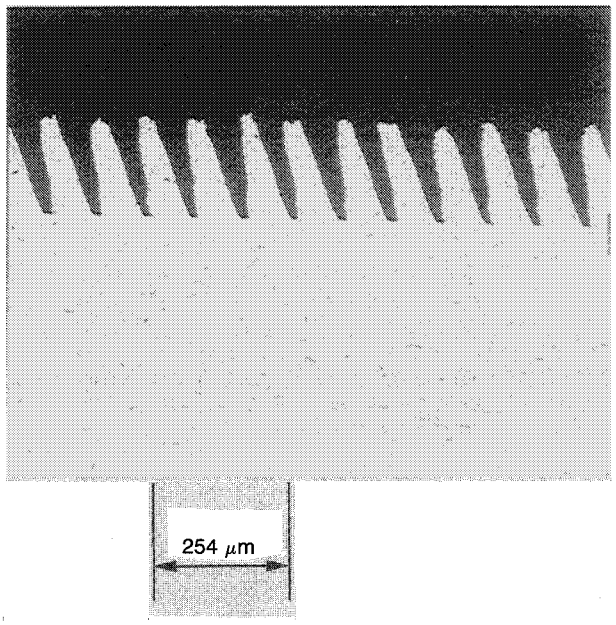

Fig. 7 Micrograph of the microgroove surface.

Inside the tank a condenser was connected to its coolant supply by fittings which passed through the cover plate. At the bottom of the condenser, a baffle was welded so that the condensed liquid would be directed to the liquid pool away from the grooved surface. City water was used as the condenser coolant. A flowmeter was used to control the water flow rate to the condenser to keep the system stabilized at a specified saturation condition. To monitor the saturation condition in the tank, a pressure gauge was installed on the cover plate. A thermocouple was also installed in the vapor region to monitor the vapor temperature in the tank.

The dimensions of the copper slab was 127 × 25.4 × 101.6 mm, whereas the length of the groove was 25.4 mm. At each of five locations along the groove channel, an array of three thermocouples was embedded in the copper slab to measure the temperature distribution. These thermocouples were located at 2.5, 7.6, and 15.2 mm below the grooved surface, respectively. Temperature readings were taken using a Fluke digital readout connected through an Omega thermocouple switch. The V grooves were 64 μm wide and 190 μm deep. Half the apex angle of a groove was 9.35 deg. The density of the grooves was 110/cm. Figure 7 shows a micrograph of the grooved surface.

The tank was mounted on a wood box attached to a supporting frame which made it possible to orient the grooved surface at different angles relative to horizontal. Acetone and methanol were used as the test liquids. Experiments were carried out at or near atmospheric pressure.

Experimental Procedure and Results

The experimental procedure was as follows. With the axis of the groove inclined at a predetermined angle with respect to gravity, the tank was filled with a test liquid until it touched the lower edge of the grooved surface. When heat was supplied, liquid was pumped up along the grooves by the capillary pressure gradient and evaporated. The vapor generated in this manner was then condensed and fell back into the liquid pool. For a preset power rate, the flow rate through the condenser was adjusted such that the vapor temperature was stabilized at the saturation temperature of the test liquid at or near atmospheric pressure. It generally required about 30 min to stabilize the system.

When the system was stabilized at a desired condition, temperature readings were taken. The data were first reduced by defining a finite element around each thermocouple in the copper slab and calculating the energy balance for each element. Heat conduction from one element to another can be determined from the obtained temperatures and the distances between the thermocouples. From the energy balance calculations, the surface heat flux and superheat were obtained at those thermocouple bank locations. The mean heat flux and heat transfer coefficients for the first two surface elements determined in this manner are indicated by the " + " symbols in Figs. 8 and 9 for a typical run for methanol and acetone, respectively. The heat fluxes for the remaining three surfaces elements were close to zero, hence, they are not shown here.

There were several unexpected complexities in our experiment. In designing the experimental apparatus, we anticipated

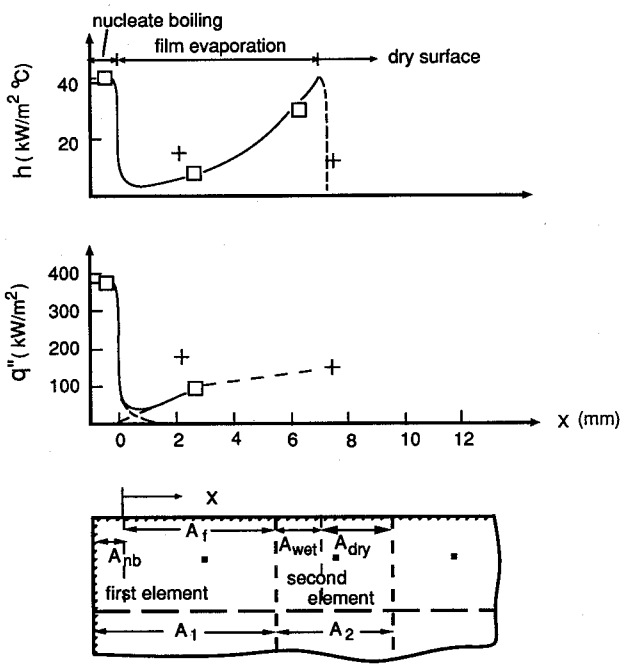

Fig. 8 Typical data for methanol with the normal of the surface at 30 deg angle relative to gravity; treatment of the nucleate boiling at the first element and the dryout at the second element.

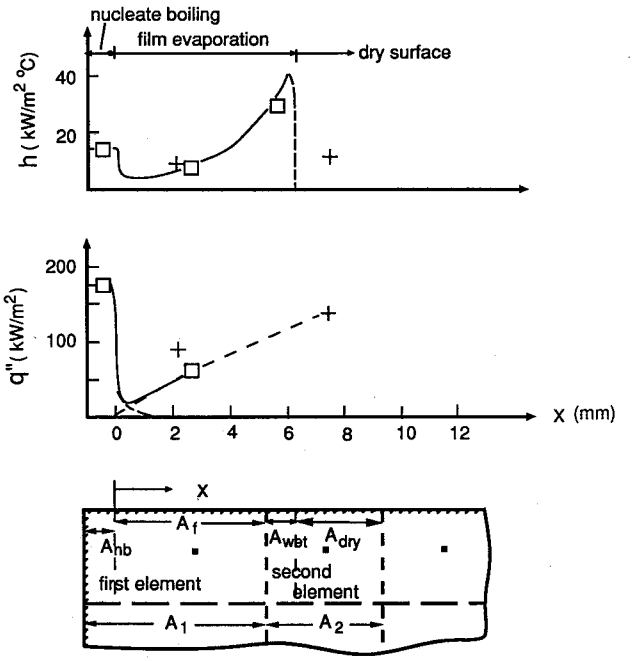

Fig. 9 Typical data for acetone with the normal of the surface at 20 deg angle relative to gravity; treatment of the nucleate boiling at the first element and the dryout at the second element.

that most of the copper surface would be wetted by liquid and that film evaporation would therefore occur over most of the grooved surface. We found, however, that the nature of our apparatus was such that accurate data could be obtained only at higher heat flux levels, which resulted in some nucleate boiling at the immersed end of the surface and a dryout of the liquid film only a short distance along the surface. Despite this, detailed analysis of the data allowed us to deduce the film-evaporation contribution to the overall heat transfer from the surface (see Appendix).

Based on the method described in the Appendix, heat transfer coefficient data for the film-evaporation region were obtained. These are shown in Figs. 8 and 9 as the square symbols. The theoretically predicted heat transfer coefficient variation in the film-evaporation region is also shown respectively in Figs. 8 and 9 as a solid curve. This result of h is based on the groove geometry, fluid properties, the assumed q'' profile (the straight dash lines in q''-x plot in Figs. 8 and 9), and the constants $A = 1 \times 10^{-11}\ Pa(m)^B$ and $B = 3.0$. The reason for choosing these values for A and B will be discussed shortly. Note that the theoretical prediction is valid only in the film-evaporation region. A sudden dropoff of h occurs when dryout occurs. This trend is indicated by the dashed curve in the h-x plot.

It can be seen from Figs. 8 and 9 that the experimentally determined film evaporation heat transfer coefficients for methanol and acetone reached as high as 30 kW/m^2° C. The superheat obtained during the experiments ranged from 5–10° C, which was relatively high for film evaporation.

Figure 10 shows the Nu and Ψ^{-1} data from the experiments. The corresponding values of Nu were determined from h. Meanwhile, using the assumed sectionally linear q'' profile for film-evaporation region, Ψ was computed from Eq. (9) for each data point. Note that the parameter K in Eq. (3) is approximated here by $K = 10.94$ for $\theta = 10$ deg, given in Ref. 12 (since in our tests $\theta = 9.35$ deg). The best fit to the data, which are based on the analytical model, are also shown in Fig. 10 for methanol and acetone. The values of A and B obtained from the best fit of the data are $A = 1 \times 10^{-11}\ Pa(m)^B$ and $B = 3.0$. These values were used when determining the theoretical h variations as shown in Figs. 8 and 9. It can be seen that the theoretical prediction shows the right trend and agrees fairly well with the experimental results. In their study, Potash and Wayner[6] have presented two sets of values for A and B for carbon tetrachloride on glass: $A = 1.702\ Pa(m)^B$ and $B = 0.61$ for the extremely thin films ($\delta \leq 7.28 \times 10^{-3}\mu m$) and $A = 0.61 \times 10^{\times 19}\ Pa(m)^B$ and $B = 3.0$ for the relatively thick ones ($\delta > 7.28 \times 10^{-3}\mu m$). Our experimental data indicate that the film thickness ranges from 2–20 μm. Hence, the value of $B = 3.0$ was chosen in this study. However, the value of A obtained from the best fit of our data is considerably different than the value of $A = 0.61 \times 10^{-19}\ Pa(m)^B$ recommended in Ref. 6.

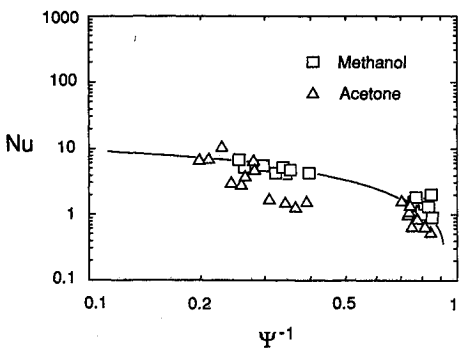

Fig. 10 Comparison of the experimentally determined relation between Nu and Ψ^{-1} vs that predicted by the analytical model. The solid line is the best fit to the experimental data, with the constants in the disjoining pressure equation to $A = 1 \times 10^{-11}\ Pa(m)^B$ and $B = 3.0$.

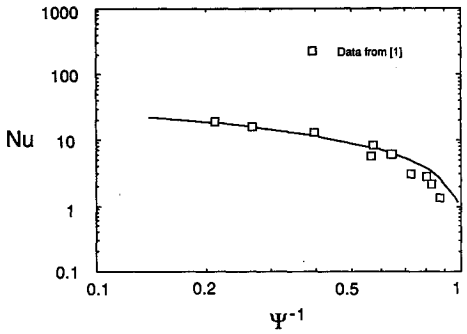

Fig. 11 Comparison of the data of Holmes and Feild[1] with predictions of the model.

In Fig. 11, some experimental data for evaporation of ammonia on a microgroove surface presented in Ref. 1 are shown along with our theoretical prediction. From personal correspondence with the authors of Ref. 1, the heat flux profile and the geometric dimensions were obtained for their surface. The data were then transformed to Nu and Ψ^{-1} according to the procedures in the model, with $K = 10.15$ for $\theta = 20$ deg presented in Ref. 12. Very good agreement between these experimental data and the analytical prediction can be observed with $A = 0.61 \times 10^{-13}\ Pa(m)^B$ and $B = 3.0$.

It should be noted that very different values of the parameter A were used in our theoretical prediction for our experimental system in Ref. 1. This is not completely surprising since the working fluids, as well as the materials used for the grooved surface, are different in these two systems. In the experiments conducted in Ref. 1, the combination of ammonia and aluminum were selected. Ammonia, which is a polar molecule, has different properties than methanol and acetone which are nonpolar. Hence, in general, it is expected that the parameters A and B in the disjoining pressure relation will depend on the combinations of working fluid and surface material.

Discussion

In our analysis, we assumed that the thin film extends to the top of the groove side wall and that q''_L is uniform. Values of A and B obtained by fitting our experimental data and the data in Ref. 1 indicate that δ varies very little along V-groove walls. This is consistent with the uniform q''_L idealization adopted in the analysis. It should also be mentioned that R_m, the interfacial thermal resistance, as derived by Sukhatme and Rohsenow,[13] is neglected in our analysis. We have calculated R_m for several conditions, using the equation given in Ref. 15, and found that it would be comparable to R_δ when the film is thinner than 0.5 μm (with $\bar{\sigma} = 0.04$). If $\bar{\sigma} = 1.0$, the film should be even thinner in order for R_m to be comparable to R_δ. However, for most of the cases of interest here, the film thickness was computed to be in the range of 2–20 μm. Since these estimates indicate that R_m is generally small compared to R_δ, this suggests that it is appropriate to neglect the interfacial resistance in this analysis. As in additional check, the equilibrium film thickness was also calculated for several conditions. The results indicate that the film thickness obtained in our experiments is larger than the equilibrium film thickness, indicating that the thin film was evaporating.

It is worth noting that the heat conduction in the copper slab in the immediate vicinity of the V groove is not considered in the analysis, nor is the effect of the variation of the surface tension with temperature. Typical results from the experiment show that the temperature variation in the copper, from the apex of the V groove to its top edge, is no more than about 0.05°C. Hence, it appears reasonable to neglect the variation of the temperature along the V-groove wall in the copper. As for the influence of the surface-tension variation with temper-

ature, a 10°C variation of temperature results in about an 8% variation of σ for acetone. This implies that variations of σ in this system are sufficiently small that it is reasonable to idealize it as being constant.

It is also interesting to note that, when the gravity effect on the film and intrinsic meniscus is neglected along the groove channel (in the x direction), the following closed integral form for Ψ can be obtained:

$$\Psi = \left[\Psi_0^{-3} - 3\int_0^{\eta} \int_{\eta}^{\eta_{\max}} Q''(\eta)\, d\eta\, d\eta \right]^{-1/3} \tag{27}$$

Moreover, for very small grooves such as those used in the present study, the film thickness varies very little on the groove side walls (in the z direction) so that the mean film thickness is almost equal to the maximum film thickness. For these circumstances, the relation between Nu and Ψ^{-1} can be simplified to

$$Nu \approx (2z_m N)w\left(\frac{Aw}{\sigma}\right)^{-1/B} (\Psi^{-1})^{-1/B} \tag{28}$$

This simpler but more approximate version of the model may be more useful for the design of microgroove evaporator surfaces since the effects of fluid properties and surface geometry variables are more explicit in the resulting correlation. Calculations using this form of the model and the full model indicate that there is little loss in accuracy associated with neglecting gravity effects.

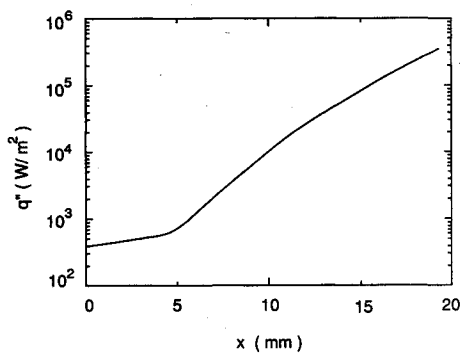

Fig. 12 An assumed heat flux distribution used in the parametric study.

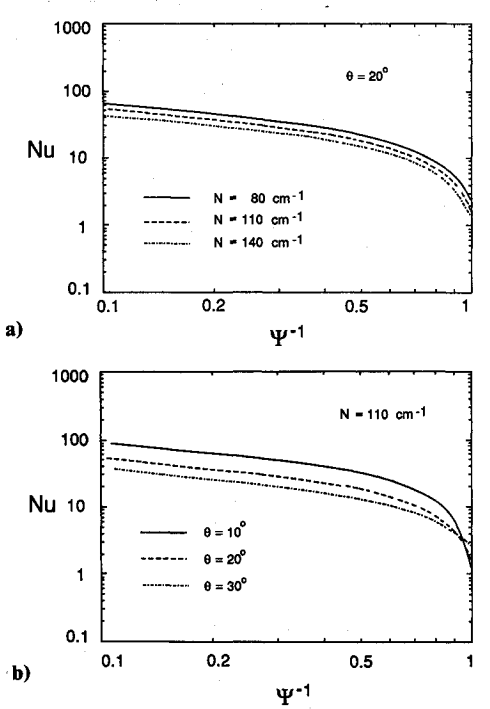

Fig. 13 Effect of varying the geometric parameters of the triangular microgroove surface on the relation of Nu vs Ψ^{-1}. The results shown are for ammonia with a) varying N and fixed θ, and b) varying θ and fixed N.

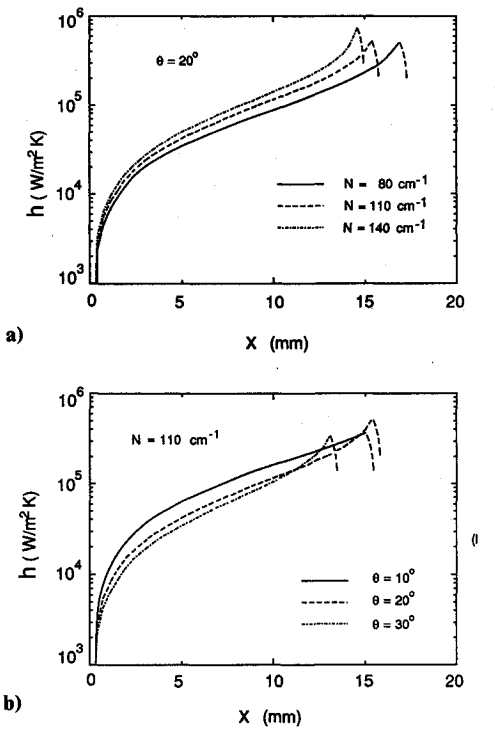

Fig. 14 Effect of varying the geometric parameters of the triangular microgroove surface on the heat transfer coefficient. The results shown are for ammonia with a) varying N and fixed θ, and b) varying θ and fixed N.

A parametric study was also conducted in order to predict the effect of the geometric parameters on the heat transfer performance of a microgroove surface. In the parametric study, we assume that there is no space between the grooves (i.e., $1/N = 2w$ in Fig. 4). We also assume that the following remain fixed: the fluid properties $q''(x)$ and the length of the groove channel L. Among the fixed parameters, $q''(x)$ was chosen to be one that is typically encountered in the grooved surface heat-pipe applications (shown in Fig. 12), the working fluid to be ammonia at a pressure of 880 kPa, and L to be 19.2 mm.

Since the groove density N is related directly to the groove width $2w$, only two variables can be changed, which we chose to be N and half-groove angle θ. We specifically examined the following two cases: 1) fixed θ with varying N, and 2) fixed N with varying θ. The resulting variations in the relation between Nu and Ψ are shown in Figs. 13a and 13b. In addition, variations in $h(x)$ are shown in Figs. 14a and 14b.

It should be noted that the preceding results were based on the assumption that $q''(x)$ would not change when varying the geometric parameters. In many heat-pipe applications, $q''(x)$ would, in fact, vary with changes in the surface geometry.

Concluding Remarks

In this study, we presented an approximate model to investigate the mechanism of film evaporation in a V-groove channel. In this model, the heat transfer in the intrinsic meniscus is neglected, implying that film evaporation in the extended meniscus is the dominant mechanism. A relation between the Nusselt number and a parameter Ψ developed in the model can be determined numerically from the resulting set of nondimensional equations.

The experiments conducted as part of this study to evaluate the theoretical model were not as definitive as we had initially hoped. Because of the assumptions invoked in the data reduction to account for the effects of nucleate boiling and surface dryout, the uncertainty in the film evaporation heat transfer coefficients determined from the data is relatively high. Nevertheless, the trends for both fluids tested agree well with those predicted by the model. Although these data do not completely validate the model, they do support the contention that it provides a realistic treatment of the flow and heat transfer.

It is perhaps more significant that the model predictions agree well with heat transfer data for film evaporation of ammonia on a different microgroove surface obtained independently by Holmes and Feild.[1] The good agreement with these data appears to be the most convincing evidence supporting the hypothesis, stated in our model, that disjoining pressure effects are important. The good agreement between predictions of this approximate model and the data for different fluids suggests that it may be a useful tool for evaluating the performance of microgroove evaporators for heat-pipe applications. It is clear, however, that more information about the disjoining pressure effects in thin films is needed to apply this model widely to real systems.

A parametric study was also conducted to explore the effect of geometric parameters on the heat transfer performance. It can be seen from the results (Figs. 14a and 14b) that, when the groove density is fixed, the heat transfer performance is enhanced by decreasing the apex angle of the grooves (making the grooves deeper), and when the apex angle of the grooves is fixed, the heat transfer coefficient increases with increasing groove density.

Appendix

In the section on Experimental Procedure and Results, it was mentioned that our experiment had some unexpected complexities, such as the nucleate boiling at the leading edge and the early dryout of the grooved surface. In this section, we describe a method to deduce the heat transfer data due to film-evaporation mechanism alone, by properly accounting for the effects of nucleate boiling and dryout.

During the experiment, we found that there is a minimum surface heat flux level for our system below which the temperature differences in the copper slab are so low that uncertainty in the thermocouple readings results in unacceptably high uncertainty in the experimentally determined values of the heat transfer coefficient. We therefore had to limit our tests to relatively higher heat flux levels. For applied heat fluxes above this minimum value, the capillary-driven flow in the grooves could sustain the film-evaporation cooling over about the first 1 cm of the surface. The measured heat flux at the thermocouple banks further along the grooved surface was virtually zero. Consequently, we could obtain heat transfer coefficient data only for the first two thermocouple bank locations along the grooved surface.

Another complicating factor became apparent when, for some of the runs, we visually observed the vaporization process in the tank using a clear plastic top cover plate. During these experiments, we saw some nucleate boiling along the immersed edge of the copper slab. The sizes of the bubbles formed were visually observed to be about 2 mm in diameter. Beyond the lower edge, no nucleate boiling was visible, which suggested that heat transfer in this region was solely due to film evaporation.

It was not surprising that nucleate boiling existed at the lower edge, because the grooves could provide nucleation sites. When these sites are fully immersed in liquid, film evaporation cannot occur. In many models of nucleate boiling heat transfer at isolated nucleation sites (see Refs. 14 and 15, for example), it is often argued that the influence of nucleate boiling is confined to a radius of no more than one bubble diameter. Therefore, in our experiments, it is plausible to assume that the region of nucleate boiling influence on the copper surface equals about the radius of a bubble, i.e., within 1 mm of the lower edge.

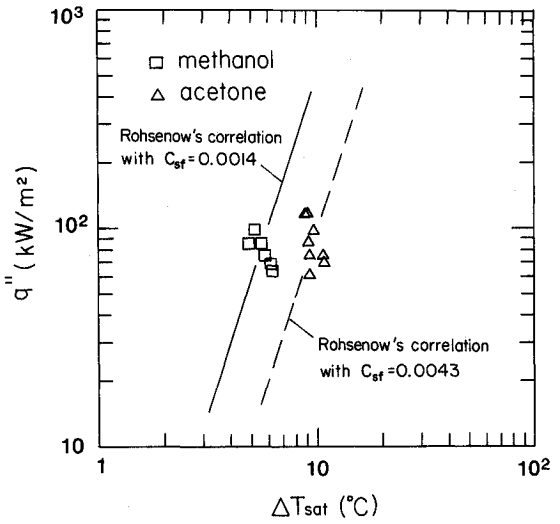

Fig. A1 Pool boiling data for the grooved surface with methanol and acetone.

Because of the presence of nucleate boiling and dryout, the mean heat transfer coefficient values indicated in Figs. 8 and 9 by the "+" symbols represent the effects of more than one mechanism. To reduce the data in a way that accounts for these additional features, the following procedure was used.

Based on our observations regarding the region of nucleate boiling influence, we assume that the first 1 mm of the first surface element (see Figs. 8 and 9) transferred heat by nucleate boiling alone and that the portion of this element beyond 1 mm transferred heat by film evaporation alone. This transition between these two mechanisms is, in fact, similar to that observed in saturated convective boiling in round tubes at low heat flux, where a transition from saturated nucleate boiling to annular film-flow evaporation is often observed.

Based on the preceding idealizations, an energy balance for the first surface element in Figs. 8 and 9 is given by

$$q''_{nb} A_{nb} + q''_{f_1} A_{f_1} = \overline{q''_1} A_1 \tag{A1}$$

where $\overline{q''_1}$ is the mean heat flux for this element. To obtain the pool boiling data for the grooved surface with each test liquid, thereby determining the q''_{nb} in Eq. (A1), several runs were conducted with the entire surface immersed in the liquid. The limited-pool boiling data obtained were used to estimate the nuclear boiling curve based on Rohsenow's correlation for each fluid, as shown in Fig. A1. When calculating values of q''_{nb} and h_{nb} for the film-evaporation runs, the superheat at the immersed edge was extrapolated from the subsurface temperatures measured at the other thermocouple bank locations. Equation (A1) was then used to determine q''_{f_1} the mean heat flux associated with film evaporation over the portion of this first element beyond 1 mm from the edge. From q''_{f_1} and the measured superheat in the film-evaporation region, the heat transfer coefficient in the film-evaporation region h_{f1} was determined. These inferred values of heat transfer coefficient and heat flux are shown as the square symbols over the first element in Figs. 8 and 9. From the results, it is estimated that nucleate boiling typically contributes 20–30% of the total heat transfer and film evaporation contributes 70–80%.

In the experiments conducted with this grooved surface, the results generally indicated that no evaporative cooling occurred beyond a distance of about 9 mm from the immersed end of the grooved surface. This suggested that the capillary-wicking mechanism was unable to supply a steady flow of

liquid to the surface beyond this location when evaporation occurred over the first 9 mm. Apparently, the intrinsic meniscus and extended meniscus were completely evaporated away over the interval $0<x<9$ mm, implying that the grooves were essentially dried out beyond this location. Visually, however, reflection of light from the surface beyond this location made the surface appear shiny, suggesting that the surface was covered with an absorbed equilibrium liquid film which was not evaporating. For practical heat transfer purposes, this portion of the surface was dry, and hence we refer to it as such.

Because of the partial dryout in the second element, a two-component energy balance was also made for this element, as can be seen in Fig. 8. The equation for the energy balance can be written as

$$q''_{f_2} A_{\text{wet}} + q''_{\text{dry}} A_{\text{dry}} = \overline{q''_2} A_2 \tag{A2}$$

Assuming that the superheat is constant for the entire second element, and that h_{dry} is negligible compared to h_{f_2}, it follows directly from the preceding relation that the film-evaporation heat transfer coefficient in the wetted portion h_{f_2} can be obtained from the following equation

$$h_{f_2} A_{\text{wet}} = \overline{h_2} A_2 \tag{A3}$$

where $\overline{h_2} = \overline{q''_2}/(T_{W2} - T_{\text{sat}})$. The area A_{wet} is easily determined if the dryout location is known.

The dryout location was not determined directly in our experiments. Rather, it was inferred from our results in the following manner. The heat flux variation in the first element (see Fig. 8) was extended into the second by assuming a linear profile which fit the value of q''_{f_1} determined for the first element and $\overline{q''_2}$, the mean heat flux for the second element. This heat flux variation, which is expected to be a reasonable approximation of the actual variation of the heat flux along the surface, was used to determine the dryout location of the analytical model described in the preceding section.

Acknowledgments

Support for this research by Lockheed Missiles and Space Company and the National Science Foundation under Grant CBT-8451781 is gratefully acknowledged. We are also indebted to Roland Holmes for his help in initiating the experimental portion of this project.

References

[1]Holmes, H. R., and Feild, A. R., "The Gas-Tolerant High-Capacity Tapered Artery Heat Pipe," AIAA Paper 86-1343, June 1986.

[2]Renk, F. J., and Wayner, P. C., Jr., "An Evaporating Ethanol Meniscus: Pt. I, Experimental Studies," *Journal of Heat Transfer*, Vol. 101, Feb. 1979, pp. 55–58.

[3]Cook, R., Tung, C. Y., and Wayner, P. C., Jr., "Usage of Scanning Microphotometer to Determine the Evaporative Heat-Transfer Characteristics of the Contact Line Region," *Journal of Heat Transfer*, Vol. 103, May 1981, pp. 325–330.

[4]Wayner, P. C., Jr., Tung, C. Y., Tirumala, M., and Yang, J. H., "Experimental Study of Evaporation in the Contact Line Region of a Thin Film of Hexane," *Journal of Heat Transfer*, Vol. 107, Feb. 1985, pp. 182–189.

[5]Mirzamoghadam, A., and Catton, I., "Holographic Interferometry Investigation of Enhanced Tube Meniscus Behavior," *Journal of Heat Transfer*, Vol. 110, Feb. 1988, pp. 208–213.

[6]Potash, M. L., Jr., and Wayner, P. C., Jr., "Evaporation from a Two-Dimensional Extended Meniscus," *International Journal of Heat and Mass Transfer*, Vol. 15, Oct. 1972, pp. 1851–1863.

[7]Wehrle, V. A., and Voulelikas, G., "Evaporation from a Two-Dimensional Meniscus," *AIAA Journal*, Vol. 23, 1985, pp. 309–313.

[8]Schneider, G. E., Yovanonich, M. M., and Wehrle, V. A., "Thermal Analysis of Trapezoidal Grooved Heatpipe Evaporator Walls," *Progress in Astronautics and Aeronautics: Thermophysics of Spacecraft and Outer Planet Entry Probes*, edited by A. M. Smith, Vol. 56, AIAA, New York, 1977, pp. 69–83.

[9]Edwards, D. K., Balakrishnan, A., and Catton, I., "Power-Law Solutions for Evaporation from a Finned Surface," *Journal of Heat Transfer*, Vol. 96, Aug. 1974, pp. 423–425.

[10]Holm, F. W., and Goplen, S. P., "Heat Transfer in the Meniscus Thin-Film Transition Region," *Journal of Heat Transfer*, Vol. 101, 1979, pp. 543–547.

[11]Vasiliev, L. L., Abramenko, A. N., and Konev, S. V., "Heat Transfer of a Liquid Boiling and Evaporating on a Capillary and Porous Surface," *Proceedings of the 6th International Heat Transfer Conference*, Paper No. FB-5, Vol. 1, 1976, pp. 299–304.

[12]Ayyaswamy, P. S., Catton, I., and Edwards, D. K., "Capillary Flow in a Triangular Groove," *Journal of Applied Mechanics*, Vol. 41, June 1974, pp. 332–336.

[13]Sukhatme, S. P., and Rohsenow, W. M., "Heat Transfer During Film Condensation of a Liquid Metal Vapor," *Journal of Heat Transfer*, Vol. 88, 1966, pp. 19–28.

[14]Mikic, B. B., and Rohsenow, W. M., "A New Correlation of Pool Boiling Data Including the Effect of Heating Surface Characteristics," *Journal of Heat Transfer*, Vol. 91, May 1969, pp. 245–251.

[15]Van Strahlen, S. J. D., "The Boiling Paradox in Binary Liquid Mixtures," *Chemical Engineering Science*, Vol. 25, Jan. 1970, pp. 149–171.